

Quantum theory of nondegenerate four-wave mixing in semiconductors

A. E. Paul

Department of Physics, University of Arizona, Tucson, Arizona 85721

M. Lindberg, S. An, and M. Sargent III

Optical Sciences Center, University of Arizona, Tucson, Arizona 85721

S. W. Koch

Department of Physics and Optical Sciences Center, University of Arizona, Tucson, Arizona 85721

(Received 26 February 1990)

A quantum theory of nondegenerate four-wave mixing is developed and applied to study a highly excited semiconductor resonator operating below or near the laser threshold. It is found that total carrier-density pulsations allow coherent effects in semiconductors despite the rapid decay of the electron-hole correlations. The output spectrum for a nondegenerate four-wave mixing intracavity experiment is computed and squeezing in the sidemode spectrum is predicted.

I. INTRODUCTION

Ever since four-wave mixing (FWM) was first proposed by Yuen and Shapiro¹ (and later by Yurke²) as a way to produce squeezed states of light, the subject of FWM has attracted a great deal of attention.^{3,4} While the majority of theoretical work in this area has dealt primarily with FWM in two-level systems, multiwave mixing in semiconductor materials has also been considered.⁵⁻⁷ In spite of the fact that buildup of the side modes in multiwave mixing relies on spontaneous emission to occur, virtually all theories of these effects in bulk materials have been semiclassical. The present paper gives a derivation of the quantized nondegenerate four-wave mixing (NDFWM) coefficients for a highly excited semiconductor material, explicitly taking into account quantum-noise processes.

In order to analyze the effects of multiwave mixing in semiconductors, we consider the situation where the optical field consists of one or two weak probe fields and a strong pump field. The carrier-density pulsations coherently scatter light from the strong mode into the weak modes, with the properties of these coherent effects depending upon the nonlinear response of the medium. In most theoretical descriptions of the optical properties of semiconductors, one supposes that the optical response of a highly excited semiconductor can be computed using a linear response theory, for which the material parameters are renormalized and depend parametrically on the electron-hole pair density.⁸⁻¹¹ This approach is best justified under quasiequilibrium conditions in the electron-hole system, which is typically established in a few hundred femtoseconds through carrier-carrier and carrier-phonon scattering. The dominant Coulomb scattering causes the electrons and holes to rapidly reach a quasithermal equilibrium where the electrons and holes are then described by Fermi-Dirac distributions within their respective bands. After reaching quasiequilibrium,

the final interband relaxation due to radiative or nonradiative recombination of electron-hole pairs is relatively slow, typically occurring within hundreds of picoseconds up to a few nanoseconds. Therefore if we study processes on time scales of picoseconds the fast relaxation dynamics of the carriers may be adiabatically eliminated, and the field-matter coherence is then related to total carrier-density fluctuations rather than the more rapid fluctuations of the individual k states of the electrons and holes. The details of the calculations are carried out in the Appendix where we follow methods inspired by standard two-level calculations to derive a set of coupled-mode equations from which we calculate NDFWM spectra. The coupled-mode equations are then used to construct the appropriate two-time correlations from which we calculate the output field and the amount of squeezing in the output field resulting from an intracavity NDFWM experiment.

II. MODEL

Nondegenerate four-wave mixing in a semiconductor medium involves the coupling of two pump photons with two weak-field photons via the nonlinear semiconductor medium. The semiconductor is placed in an optical cavity and subjected to an external coherent pump beam of frequency ν_2 . Carriers are incoherently introduced into the semiconductor via an injection current or by optical pumping at a frequency far above the band gap. The coherent pump is tuned symmetrically between two adjacent cavity modes ν_1 and ν_3 as shown in Fig. 1. The strong mode is treated semiclassically while the two sidemodes are treated quantum mechanically.¹²

To describe the electrons and holes in the medium we use the generalized Bloch equations for semiconductors as derived in Ref. 13. These equations may be simplified by noting that the rapid intraband scattering destroys electron-hole correlations on a 100-fs time scale. Provid-

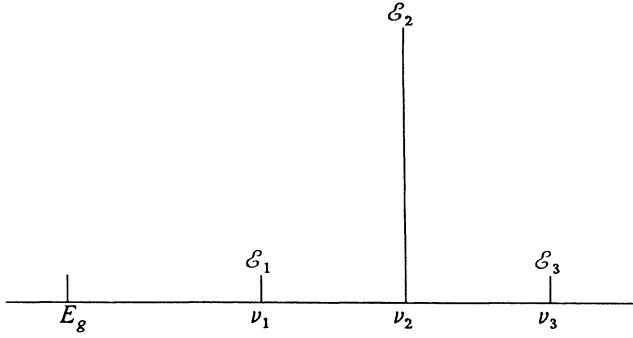


FIG. 1. Spectrum of three-mode field relative to the unrenormalized band gap E_g . Modes with frequencies ν_1 and ν_3 are weak (nonsaturating), while the mode ν_2 is allowed to be arbitrarily intense limited only by the constraints of the quasiequilibrium approximation.

ing the field does not vary much in a carrier-carrier scattering time, the rapid dephasing causes electrons and holes to relax into quasithermal equilibrium where the intraband carrier distributions are Fermi-Dirac distributions. In this limit, we neglect all Coulomb effects except that the system is in the quasiequilibrium state due to Coulomb intraband scattering. In the quasiequilibrium regime the properties of the system are parametrically related to the total carrier density, where the details of the carrier generation are of no interest as long as the generation of carriers due to the coherent pump does not interfere with the rapid thermalization process. In this regime one obtains a simple rate equation for the total electron-hole-pair density

$$\frac{\partial N}{\partial t} = -\frac{N}{\tau} + \lambda_p + \alpha(\nu, N) \frac{I(\nu)}{\hbar\nu}, \quad (1)$$

where τ is the interband recombination time, and the terms on the right-hand side describe interband recombination, incoherent carrier generation, and optical carrier generation through light absorption, respectively. This equation may be solved numerically to ensure that the number of carriers generated by the coherent pump is small in comparison with the number of incoherently generated carriers. This is a necessary condition since, in the quasiequilibrium regime, spectral hole burning is implicitly ignored via the introduction of Fermi distributions.

We derive our coupled mode equations using the standard density matrix equations of motion, which we write in the general form

$$\frac{d}{dt}\hat{\rho} = -i[\hat{H}, \hat{\rho}] + \hat{L}_{\text{inc}}(\hat{\rho}), \quad (2)$$

where \hat{H} is the total Hamiltonian and \hat{L}_{inc} is the quantum Liouville operator describing the incoherent processes.¹⁴ In the incoherent part we include spontaneous emission, electron-hole scattering, and cavity damping. The model Hamiltonian for the system is given by

$$\hat{H} = \hat{H}_e + \hat{H}_h + \hat{H}_f + \hat{H}_{\text{sc}} + \hat{H}_{\text{eh-f}}. \quad (3)$$

The first two contributions are given by the usual two-band model for noninteracting electrons and holes, namely,

$$\hat{H}_e = \sum_k \varepsilon_e(k) a_k^\dagger a_k, \quad \hat{H}_h = \sum_k \varepsilon_h(k) b_{-k}^\dagger b_{-k}. \quad (4)$$

The Hamiltonian \hat{H}_f in Eq. (3) describes the free photons of the nonsaturating modes, and is given by

$$\hat{H}_f = \nu_1 d_1^\dagger d_1 + \nu_3 d_3^\dagger d_3, \quad (5)$$

where ν_1, ν_3 are the frequencies of the side modes, and d_1^\dagger and d_3^\dagger are the corresponding creation operators. The last two terms in Eq. (3) describe the usual dipole coupling between fields and the electron-hole excitations. For the semiclassical mode we have the Hamiltonian

$$\hat{H}_{\text{sc}} = -\sum_k \mu_k \mathcal{E} e^{-i\nu_2 t} a_k^\dagger b_{-k}^\dagger + \text{H.c.}, \quad (6)$$

where μ_k is the dipole matrix element, \mathcal{E} is the field amplitude, and ν_2 is the frequency of the laser field. The explicit time dependence of Eq. (6) is eliminated by using the rotating wave approximation in which case all frequencies are given as detunings from ν_2 . Similarly the dipole coupling with the quantum-mechanical mode is given by the Hamiltonian

$$\hat{H}_{\text{eh-f}} = -\sum_k g(k) (d_1 + d_3) a_k^\dagger b_{-k}^\dagger + \text{H.c.}, \quad (7)$$

where $g(k)$ is the coupling constant. Since the quantum-mechanical field modes are damped primarily through cavity losses, the relaxation terms for the weak modes can be described by the Liouvillean¹⁵

$$\hat{L}_c(\hat{\rho}) = \kappa (2d_1 \hat{\rho} d_1^\dagger - d_1^\dagger d_1 \hat{\rho} - \hat{\rho} d_1^\dagger d_1) + (1 \leftrightarrow 3), \quad (8)$$

where κ is the cavity damping rate. A linear coupling of the electron-hole degrees of freedom to the vacuum modes leads to the Liouvillean¹⁵

$$\hat{L}_{\text{RR}}(\hat{\rho}) = \frac{\Gamma}{2} \sum_k (2b_{-k} a_k \hat{\rho} a_k^\dagger b_{-k}^\dagger - a_k^\dagger b_{-k}^\dagger b_{-k} a_k \hat{\rho} - \hat{\rho} a_k^\dagger b_{-k}^\dagger b_{-k} a_k), \quad (9)$$

where Γ is the radiative recombination rate. The nonradiative recombination is characterized with a rate γ_{NR} , assumed to be k independent. Furthermore, charge neutrality guarantees that electrons and holes have the same recombination rate.

For the expectation values of the electron-hole degrees of freedom we adopt the standard notation¹¹

$$n_e(k) \equiv \langle a_k^\dagger a_k \rangle \equiv \text{tr}(a_k^\dagger a_k \hat{\rho}), \quad (10a)$$

$$n_h(k) \equiv \langle b_{-k}^\dagger b_{-k} \rangle \equiv \text{tr}(b_{-k}^\dagger b_{-k} \hat{\rho}), \quad (10b)$$

$$p(k) \equiv \langle b_{-k} a_k \rangle \equiv \text{tr}(b_{-k} a_k \hat{\rho}). \quad (10c)$$

In quasiequilibrium these expectation values are determined essentially by Coulomb scattering, where the populations are given by Fermi-Dirac distributions, and the polarization takes the form

$$p(k) = i\mu_k \mathcal{E} \mathcal{D}_2^*(k) [1 - f_e(k) - f_h(k)], \quad (11a)$$

where

$$\begin{aligned} \mathcal{D}_2(k) &= \{\gamma - i[\varepsilon_e(k) + \varepsilon_h(k) - \nu_2]\}^{-1} \\ &\equiv \{\gamma - i[\omega(k) - \nu_2]\}^{-1}, \end{aligned} \quad (11b)$$

and γ is the intraband Coulomb scattering rate. In general, the equation for the polarization is modified by additional many-body effects,⁸⁻¹¹ but since γ is the largest relaxation rate in the system, we assume that the polarization adiabatically follows the field fluctuations and approximate damping of the polarization with a single damping constant.

III. COUPLED-MODE EQUATIONS

The equation of motion for the total density operator is given by Eq. (2). We may calculate the reduced field density operator, which yields the time dependence of the two quantized fields, by tracing the total density operator over the electron-hole degrees of freedom. Assuming that all field amplitudes vary little in the time $1/\gamma$, we may solve the semiconductor equations of motion in steady state since in this limit the electron-hole polarization adiabatically follows the field. Using these solutions we then obtain the slowly varying field-density operator equation of motion

$$\begin{aligned} \frac{d}{dt} \hat{\rho}_f &= -A_1(\hat{\rho}_f d_1 d_1^\dagger - d_1^\dagger \hat{\rho}_f d_1) - B_1(d_1^\dagger d_1 \hat{\rho}_f - d_1 \hat{\rho}_f d_1^\dagger) \\ &+ C_1(d_1^\dagger d_3^\dagger \hat{\rho}_f - d_3^\dagger \hat{\rho}_f d_1^\dagger) + D_1(\hat{\rho}_f d_3^\dagger d_1^\dagger \\ &- d_1^\dagger \hat{\rho}_f d_3^\dagger) + (1 \leftrightarrow 3) + \text{H.c.}, \end{aligned} \quad (12)$$

where $(1 \leftrightarrow 3)$ represents the same four terms as before with 1 and 3 interchanged. Of particular interest are the equations of motion for the average photon number $\langle d_1^\dagger d_1 \rangle$ and the combination tone $\langle d_1 d_3 \rangle$. Using the equation of motion for the reduced density operator, we obtain

$$\begin{aligned} \frac{d}{dt} \langle d_1^\dagger d_1 \rangle &= (A_1 - B_1 - \gamma_{\text{cav}} - i\Delta\Omega) \langle d_1^\dagger d_1 \rangle + A_1 \\ &+ (C_1^* - D_1^*) \langle d_1 d_3 \rangle + \text{c.c.}, \end{aligned} \quad (13a)$$

$$\begin{aligned} \frac{d}{dt} \langle d_1 d_3 \rangle &= (A_1 - B_1 - \gamma_{\text{cav}} - i\Delta\Omega) \langle d_1 d_3 \rangle + C_1 \\ &+ (C_3 - D_3) \langle d_1^\dagger d_1 \rangle + (1 \leftrightarrow 3). \end{aligned} \quad (13b)$$

where we have defined $\Delta\Omega$ as the detuning of the pump mode from the nearby passive-cavity mode, and γ_{cav} is the total loss in the cavity, including internal losses. The equation of motion for $\langle d_3^\dagger d_3 \rangle$ is given by Eq. (13a) interchanging the subscripts 1 and 3. The coupled equations (13a) and (13b) contain all of the information about emission and reabsorption in the system. The real part of $\bar{\alpha}_n \equiv B_n - A_n$ is the absorption coefficient of the mode n , while the imaginary part of $\bar{\alpha}_n$ is the dispersive response for mode n . The coefficient $\chi_n \equiv C_n - D_n$ is the semiclassical coupling coefficient, giving rise to the generation of mode n in the presence of the pump mode ν_2 and the conjugate mode n^* . The inhomogeneous source terms A_n and C_n arise due to the quantum mechanical noise pro-

cesses in the system. It is necessary to incorporate the quantum noise terms, and hence their correlations A_n and C_n , in order to calculate quantum features of the field, such as squeezing. In the Appendix we obtain a specific form for the coefficients A_n , B_n , C_n , and D_n . The coefficient A_n , which describes the fluorescence spectrum, is given by

$$A_n \equiv A_{n,R} + \delta A_0 + \delta A_{n,\text{pul}}, \quad (14a)$$

where $A_{n,R}$ is the Rayleigh (zeroth-order) contribution which gives a δ -function peak spectrum

$$A_{n,R} \equiv 2\pi\delta(\Delta_n) \left| \sum_k g(k) p^*(k) \right|^2. \quad (14b)$$

The second contribution δA_0 , the so-called ordinary resonance fluorescence, is given by

$$\delta A_0 = \sum_k |g(k)|^2 \mathcal{D}_2(k) f_e(k) f_h(k). \quad (14c)$$

This term is independent of the excitation mechanism, and is responsible for the large background contribution to A_n (Fig. 2). The last term $\delta A_{n,\text{pul}}$ is the coherent contribution due to the carrier-density pulsations which is given by

$$\delta A_{n,\text{pul}} = \delta A_{n,e-h} + \delta A_{n,p} + \delta A_{n,e} + \delta A_{n,h}, \quad (14d)$$

where

$$\begin{aligned} \delta A_{n,e-h} &= - \sum_k 2\mu_k \mathcal{E} g^*(k) \mathcal{D}_2^*(k) \frac{g_e(k) + g_h(k)}{(\gamma_{\text{NR}} + \gamma_e + \gamma_h - i\Delta_n)} \\ &\times \sum_{k'} \mu_{k'}^* \mathcal{E}^* g(k') \frac{\mathcal{L}(k')}{\gamma} f_e(k') f_h(k'), \end{aligned} \quad (14e)$$

$$\begin{aligned} \delta A_{n,p} &= \sum_k \mu_k \mathcal{E} g^*(k) \mathcal{D}_2^*(k) \frac{g_e(k) + g_h(k)}{(\gamma_{\text{NR}} + \gamma_e + \gamma_h - i\Delta_n)} \\ &\times \sum_{k'} |\mu_{k'} \mathcal{E}|^2 \mu_{k'}^* \mathcal{E}^* g(k') \mathcal{D}_2(k')^3 \\ &\times [1 - f_e(k') - f_h(k')]^2, \end{aligned} \quad (14f)$$

$$\begin{aligned} \delta A_{n,e} &= \sum_k \mu_k \mathcal{E} g^*(k) \mathcal{D}_2^*(k) \\ &\times \frac{g_e(k)(\gamma_{\text{NR}} + \gamma_e - i\Delta_n) - g_h(k)\gamma_h}{(\gamma_{\text{NR}} + \gamma_e + \gamma_h - i\Delta_n)(\gamma_{\text{NR}} - i\Delta_n)} \\ &\times \sum_{k'} \mu_{k'}^* \mathcal{E}^* g(k') \mathcal{D}_2(k') [1 - f_e(k')] f_e(k'), \end{aligned} \quad (14g)$$

and $\delta A_{n,h}$ is given by $\delta A_{n,e}$ with e and h interchanged. This is identical to the A_1 coefficient derived by Lindberg *et al.*¹⁶ where we have defined $\Delta_n \equiv \nu_n - \nu_2$, and $\mathcal{D}_2(k)$ is given by Eq. (11b) and $\mathcal{L}(k) = \gamma \text{Re}[\mathcal{D}_2(k)]$.

The C_n coefficient is the inhomogeneous source term for the combination tone. It is this term which is responsible for squeezing,

$$C_n = C_{n,R} + \delta C_0 + \delta C_{n,\text{pul}}, \quad (15a)$$

where $C_{n,R}$ is identical to the Rayleigh term (14b) when ν_1 and ν_3 are conjugate modes. The remaining contributions to C_n are

$$\delta C_0 = -2 \sum_k [\mu_k \mathcal{E} g^*(k)]^2 \mathcal{D}_2(k)^3 [1 - f_e(k) - f_h(k)]^2 \quad (15b)$$

and

$$\delta C_{n,\text{pul}} = \delta C_{n,e-h} + \delta C_{n,p} + \delta C_{n,e} + \delta C_{n,h}, \quad (15c)$$

where

$$\begin{aligned} \delta C_{n,e-h} = & - \sum_k 2\mu_k \mathcal{E} g^*(k) \mathcal{D}_2^*(k) \frac{g_e(k) + g_h(k)}{(\gamma_{\text{NR}} + \gamma_e + \gamma_h - i\Delta_n)} \\ & \times \sum_{k'} \mu_{k'} \mathcal{E} g^*(k') \frac{\mathcal{L}(k')}{\gamma} f_e(k') f_h(k'), \end{aligned} \quad (15d)$$

$$\begin{aligned} \delta C_{n,p} = & \sum_k \mu_k \mathcal{E} g^*(k) \mathcal{D}_2^*(k) \frac{g_e(k) + g_h(k)}{(\gamma_{\text{NR}} + \gamma_e + \gamma_h - i\Delta_n)} \\ & \times \sum_{k'} |\mu_{k'} \mathcal{E}|^2 \mu_{k'} \mathcal{E} g^*(k') \mathcal{D}_2(k')^3 \\ & \times [1 - f_e(k') - f_h(k')]^2, \end{aligned} \quad (15e)$$

$$\begin{aligned} \delta C_{n,e} = & \sum_k \mu_k \mathcal{E} g^*(k) \mathcal{D}_2^*(k) \\ & \times \frac{g_e(k)(\gamma_{\text{NR}} + \gamma_e - i\Delta_n) - g_h(k)\gamma_h}{(\gamma_{\text{NR}} + \gamma_e + \gamma_h - i\Delta_n)(\gamma_{\text{NR}} - i\Delta_n)} \\ & \times \sum_{k'} \mu_{k'} \mathcal{E} g^*(k') \mathcal{D}_2(k') [1 - f_e(k')] f_e(k'), \end{aligned} \quad (15f)$$

and the equation for $\delta C_{n,h}$ is given by $\delta C_{n,e}$ with e and h interchanged.

Next, rather than writing down the coefficients B_n and D_n what we really need is the coefficient $\alpha_n \equiv \tilde{\alpha}_n + \gamma_{\text{cav}} + i\Delta\Omega$ and the coupling coefficient χ_n . For the coupling coefficient χ_n we obtain

$$\begin{aligned} \chi_n = & \sum_k \mu_k \mathcal{E} g^*(k) \mathcal{D}_2^*(k) \frac{g_e(k) + g_h(k)}{\gamma_{\text{NR}} + \gamma_e + \gamma_h - i\Delta_n} \\ & \times 2 \sum_{k'} \mu_{k'} \mathcal{E} g^*(k') \frac{\mathcal{L}(k')}{\gamma} [1 - f_e(k') - f_h(k')]. \end{aligned} \quad (16)$$

The semiclassical absorption coefficient $\tilde{\alpha}_n$ is

$$\tilde{\alpha}_n = \alpha_{\text{inc}} + \alpha_{n,\text{coh}} = \alpha_{\text{inc}} - \chi_n, \quad (17a)$$

where

$$\alpha_{\text{inc}} = \sum_k |g(k)|^2 \mathcal{D}_2(k) [1 - f_e(k) - f_h(k)]. \quad (17b)$$

In Fig. 2(a) we plot the incoherent absorption spectrum for different carrier densities near threshold. This figure clearly shows that for large enough carrier densities the medium exhibits a region of gain (negative absorption) at

frequencies between the band edge and the chemical potential. The laser threshold for the system is defined by the gain-equals-loss condition, and in this paper we consider the situation of carrier densities below or near threshold. The effect of the coherent pump field on the probe absorption, which is partially responsible for the NDFWM process, is shown in Fig. 3. As seen in Figs. 3(a) and 3(c), the probe absorption spectrum exhibits asymmetric dips for pump frequencies either above or below the chemical potential. When the pump frequency is near the chemical potential, the coherent dip in the absorption becomes symmetric, Fig. 3(b). The asymmetry of the probe absorption is related to the fact that fluctuations in the carrier density simultaneously affect both the absorption and the index in the active region. In addition, these figures show a shift as well as a power broadening of the coherent dip for increasing pump intensities. Both of these features can be seen to originate from the dependence of the decay constants γ_e and γ_h on the pump intensity [see Eq. (A8d)].

In addition to the induced absorption gratings there are also index gratings that arise due to the presence of the strong pump field. In Fig. 4 we show the dispersive

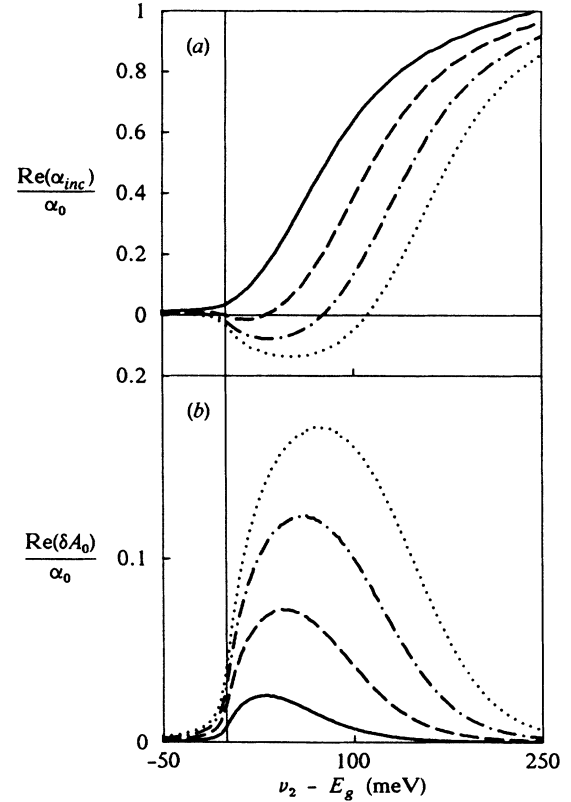


FIG. 2. Incoherent semiclassical absorption spectrum for GaAs at $T=300$ K. The carrier density $N_0=10^{18}$ (solid), 2×10^{18} cm^{-3} (dashed), 3×10^{18} cm^{-3} (dot-dashed), 4×10^{18} cm^{-3} (dotted), $\hbar\gamma=5$ meV, $\hbar\Gamma=0.0006$ meV, $\hbar\gamma_{\text{NR}}=0.0001$ meV, $m_e=1.127m$, $m_h=8.82m$, where m is the reduced effective mass. (b) The corresponding incoherent fluorescence spectrum.

response $\text{Im}(\tilde{\alpha}_1)$ for various pump frequencies. As can be seen from these figures the dispersive profile is asymmetric at all pump frequencies. Specifically, at frequencies well below (above) the chemical potential the dispersive response exhibits an asymmetric dip (peak) which shows the same type of power broadening and shift as the absorption spectrum. At pump frequencies near the chemical potential the dispersive response appears very similar to that of a two-level atom which is a consequence of the corresponding symmetric nature of the absorption spectrum. Furthermore because of the large asymmetry of the dispersion term, perfect phase matching of the

sidebands cannot be achieved in a collinear cavity configuration. This result is of importance later when we discuss the NDFWM spectrum outside the cavity.

The coupling response $|\chi_1|$, which may be thought of as the spectrum for FWM between the sidebands, is plotted in Fig. 5. This figure shows that the maximum coupling occurs at $\Delta_1=0$, that is, for degenerate four-wave mixing (DFWM). The basic shape of the coupling spectrum is the same at all pump frequencies with the peak value increasing for increasing pump frequencies and intensities. Due to contributions from both the real and imaginary parts of χ_1 , the width of the coupling spectrum

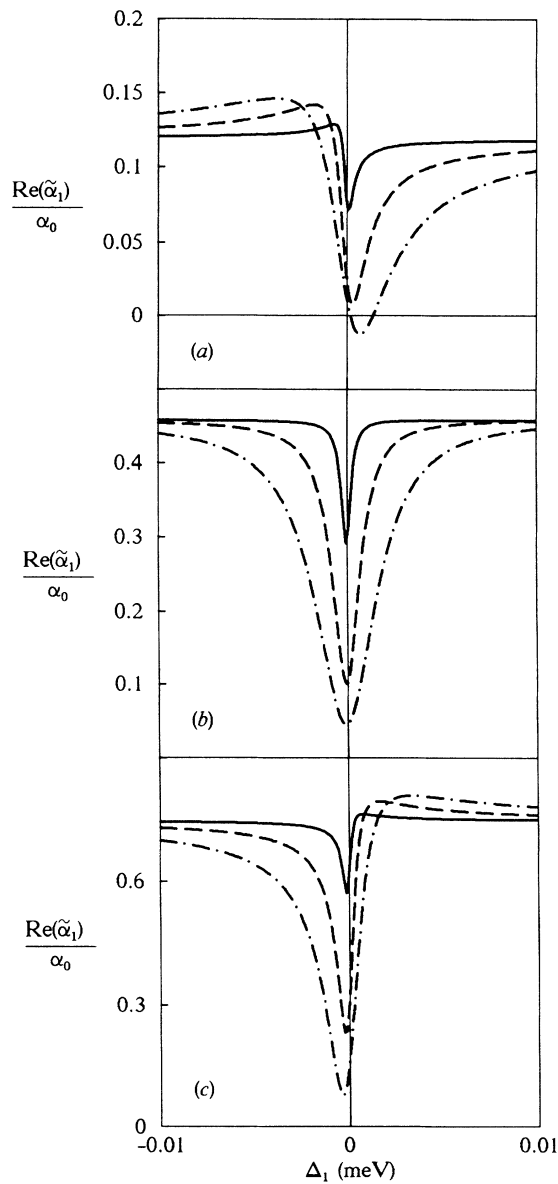


FIG. 3. Total absorption coefficient vs pump-probe detuning Δ_1 . The carrier density $N_0 = 10^{18} \text{ cm}^{-3}$, $|2\mu\mathcal{E}| = 0.1$ (solid), 0.25 (dashed), 0.4 meV (dot-dashed), $\nu_2 - E_g = 25$ meV (a), 75 meV (b), and 125 meV (c), and the rest of the parameters are the same as in Fig. 2.

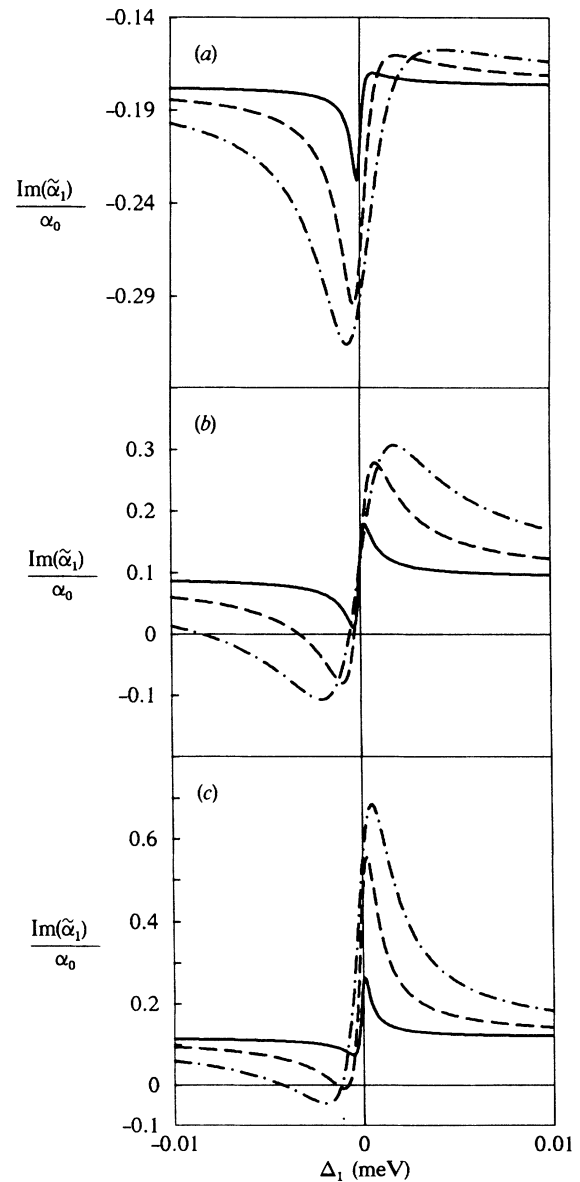


FIG. 4. Dispersive response vs pump-probe detuning Δ_1 . The carrier density $N_0 = 10^{18} \text{ cm}^{-3}$, $|2\mu\mathcal{E}| = 0.1$ meV (solid), 0.25 meV (dashed), 0.4 meV (dot-dashed), $\nu_2 - E_g = 25$ meV (a), 75 meV (b), and 125 meV (c), and the rest of the parameters are the same as in Fig. 2.

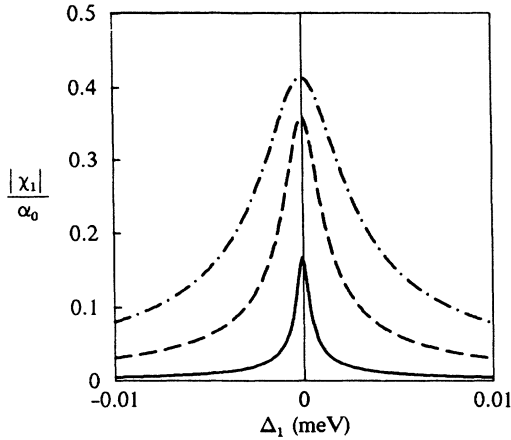


FIG. 5. Coupling response vs pump-probe detuning Δ_1 . The carrier density $N_0=10^{18} \text{ cm}^{-3}$, $|2\mu\mathcal{E}|=0.1 \text{ meV}$ (solid), 0.25 meV (dashed), 0.4 meV (dot-dashed), $\nu_2 - E_g = 75 \text{ meV}$, and the rest of the parameters are the same as in Fig. 2.

is rather large.

In addition, since the buildup of the sidemodes relies on spontaneous emission to occur, we must include the quantum noise correlations A_n and C_n . In Fig. 2(b) we show the so-called ordinary (incoherent) fluorescence spectrum δA_0 for several different carrier densities. As this figure clearly shows, the fluorescence spectrum exhibits an asymmetric shape which is basically the same at all carrier densities. While the peak of the spectrum is mainly determined by the total carrier density, the asymmetry and large width of the spectrum is due to the large intrinsic inhomogeneous broadening resulting from the dispersion of the energy bands. In Fig. 6 we plot the total fluorescence spectrum for various pump frequencies which shows that for pump frequencies far enough above the chemical potential the fluorescence spectrum exhibits a sharp peak which increases for increasing pump intensities. At pump frequencies near or below the chemical potential the fluorescence spectrum exhibits an asymmetric coherent-dip spectrum for sufficiently large Rabi frequencies. This sharp dip is attributed to the nonradiative and intensity dependent decay processes in the medium which specifically appear in the terms $\delta A_{n,e}$ and $\delta A_{n,h}$. This is reminiscent of the coherent-dip spectrum observed in two-level systems in which the population difference lifetime (T_1) greatly exceeds the dipole lifetime (T_2). The situation in semiconductors is similarly characterized by $T_1 \gg T_2$ since T_1 is essentially given by the radiative recombination time ($\approx \text{ns}$) while T_2 is characterized by the carrier-carrier scattering time ($\approx 200 \text{ fs}$).

The behavior of the phase-sensitive term C_1 is summarized in Fig. 7. The real part of C_1 is essentially the same as the coherent contribution to A_1 , which can be seen in the similarity of Eqs. (14) and (15) or equivalently Figs. 6 and 7. Because of the similarity in the real part of A_1 and C_1 , we must rely on the imaginary part of C_1 , also shown in Fig. 7, to overcome the phase insensitive

fluorescence in order to obtain squeezing. However, the coupling spectrum $|\chi_1|$ also plays an important role in the production of squeezed light. Bearing in mind that χ_1 is the coefficient for coupling between a number of photons, as opposed to the fluorescence A_1 which relates to emission of single photons, it is interesting to compare the two spectra. As pointed out by Reid and Walls,³ increased fluorescence detracts from squeezing. Thus regimes showing large FWM coupling χ_1 with minimal fluorescence A_1 are promising for the production of squeezed light. However, the spectrum of the phase-sensitive noise term C_1 has a width similar to that of the

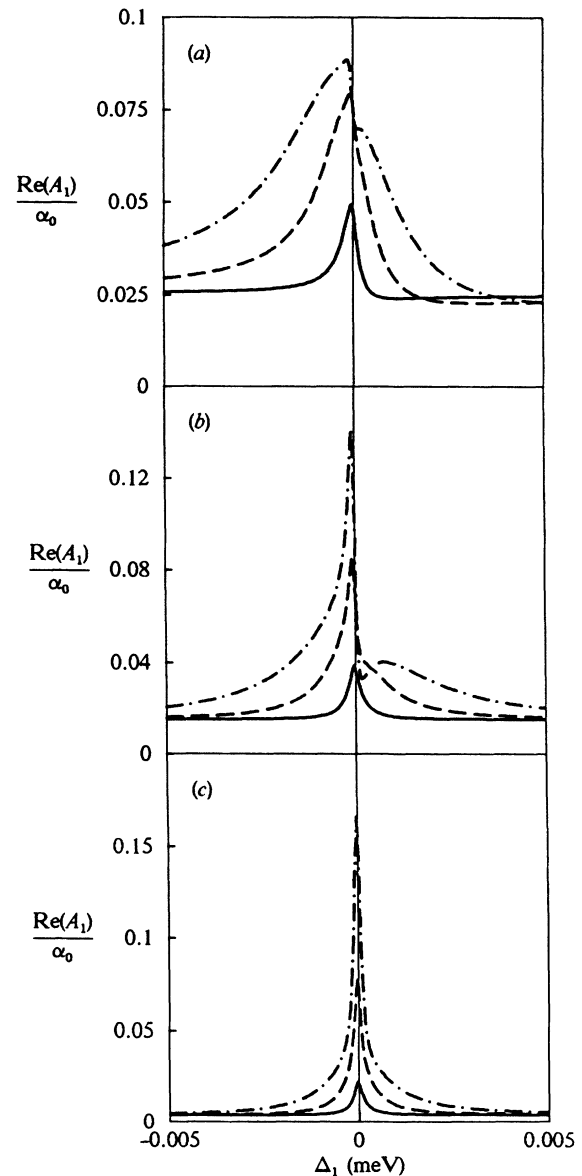


FIG. 6. Resonance fluorescence vs pump-probe detuning Δ_1 . The carrier density $N_0=10^{18} \text{ cm}^{-3}$, $|2\mu\mathcal{E}|=0.1 \text{ meV}$ (solid), 0.25 meV (dashed), 0.4 meV (dot-dashed), $\nu_2 - E_g = 25 \text{ meV}$ (a), 75 meV (b), and 125 meV (c), and the rest of the parameters are the same as in Fig. 2.

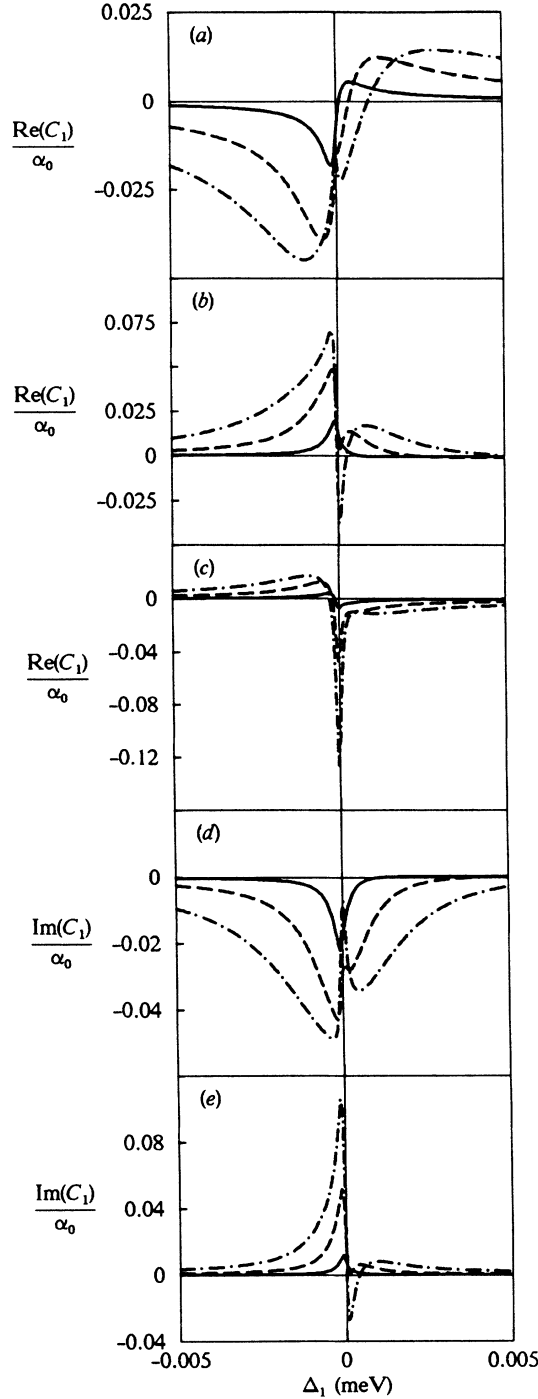


FIG. 7. Quantum coupling term vs pump-probe detuning Δ_1 . The carrier density $N_0 = 10^{18} \text{ cm}^{-3}$, $|2\mu\mathcal{E}| = 0.1 \text{ meV}$ (solid), 0.25 meV (dashed), 0.4 meV (dot-dashed), $v_2 - E_g = 25 \text{ meV}$ (a), 75 meV (b), 125 meV (c), 40 meV (d), 120 meV (e), and the rest of the parameters are the same as in Fig. 2.

fluorescence, therefore we do not expect to obtain squeezing for Δ_1 greater than the width of the fluorescence spectrum in Fig. 6.

IV. FOUR-WAVE MIXING SPECTRUM

The NDFWM spectrum may be calculated by using the quantum coupled mode equations (13a) and (13b) to solve for $\langle d_n^\dagger d_n \rangle$ and $\langle d_1 d_3 \rangle$. However, these expectation values do not represent the experimentally accessible spectra external to the cavity. In fact the detector sees a non- δ -function spectrum around each cavity mode frequency due to the time varying fluctuations about their steady-state values. To obtain the low frequency spectra of the various mode correlations let us first notice that the coupled mode equations (13a) and (13b) may be rewritten in the following form:

$$\frac{d}{dt} \langle \underline{\alpha} \underline{\alpha} \rangle = -\underline{A} \langle \underline{\alpha} \underline{\alpha} \rangle - \langle \underline{\alpha} \underline{\alpha} \rangle \underline{A}^T + \underline{D}, \quad (18)$$

where $\underline{\alpha}^T \equiv (d_1, d_1^\dagger, d_3, d_3^\dagger)$, $\langle \underline{\alpha} \underline{\alpha} \rangle \equiv \langle \underline{\alpha}(0) \underline{\alpha}^T(0) \rangle$, \underline{A} is the drift matrix derivable from Eqs. (13a) and (13b), and \underline{D} is the diffusion matrix whose elements consist of the inhomogeneous source terms of Eqs. (13a) and (13b). These matrices have the specific form

$$\underline{A} = \begin{bmatrix} \alpha_1 & 0 & 0 & -\chi_1 \\ 0 & \alpha_1^* & -\chi_1^* & 0 \\ 0 & -\chi_3 & \alpha_3 & 0 \\ -\chi_3^* & 0 & 0 & \alpha_3^* \end{bmatrix}, \quad (19)$$

$$\underline{D} = \begin{bmatrix} 0 & A_1 + A_1^* & C_1 + C_3 & 0 \\ A_1 + A_1^* & 0 & 0 & C_1^* + C_3^* \\ C_1 + C_3 & 0 & 0 & A_3 + A_3^* \\ 0 & C_1^* + C_3^* & A_3 + A_3^* & 0 \end{bmatrix}.$$

The spectral matrix can then be written as

$$\mathcal{S}_{ij}(\delta) = \int_{-\infty}^{\infty} dt e^{-i\delta t} \langle \alpha_i(t) \alpha_j(0) \rangle = [(\underline{A} - i\delta \underline{I})^{-1} \underline{D} (\underline{A}^T + i\delta \underline{I})^{-1}]_{ij}, \quad (20)$$

where \underline{I} is the identity matrix. Equation (20) has been derived by several authors,^{17,4} and the solutions for the elements of the spectral matrix are

$$\mathcal{S}_{21}(\delta) = \frac{|\alpha_3 + i\delta|^2 A_1 + |\chi_1|^2 A_3 + (\alpha_3^* - i\delta) \chi_1^* (C_1 + C_3) + \text{c.c.}}{|(\alpha_1 - i\delta)(\alpha_3^* - i\delta) - \chi_1 \chi_3^*|^2}, \quad (21a)$$

$$\mathcal{S}_{31}(\delta) = \frac{(\alpha_3^* - i\delta) \chi_3 (A_1 + A_1^*) + (\alpha_1^* + i\delta) \chi_1 (A_3 + A_3^*) + (\alpha_1^* + i\delta)(\alpha_3^* - i\delta)(C_1 + C_3) + \chi_1 \chi_3}{|(\alpha_1 - i\delta)(\alpha_3^* - i\delta) - \chi_1 \chi_3^*|^2}, \quad (21b)$$

where the expression for $\mathcal{S}_{43}(\delta)$ is given by $\mathcal{S}_{21}(\delta)$ with 1 interchanged with 3, and the remaining elements are found using the fact that $\mathcal{S}_{ji}(\delta) = \mathcal{S}_{ij}(-\delta)$. The NDFWM spectrum external to the cavity is then obtained by summing the contributions from both modes 1 and 3.

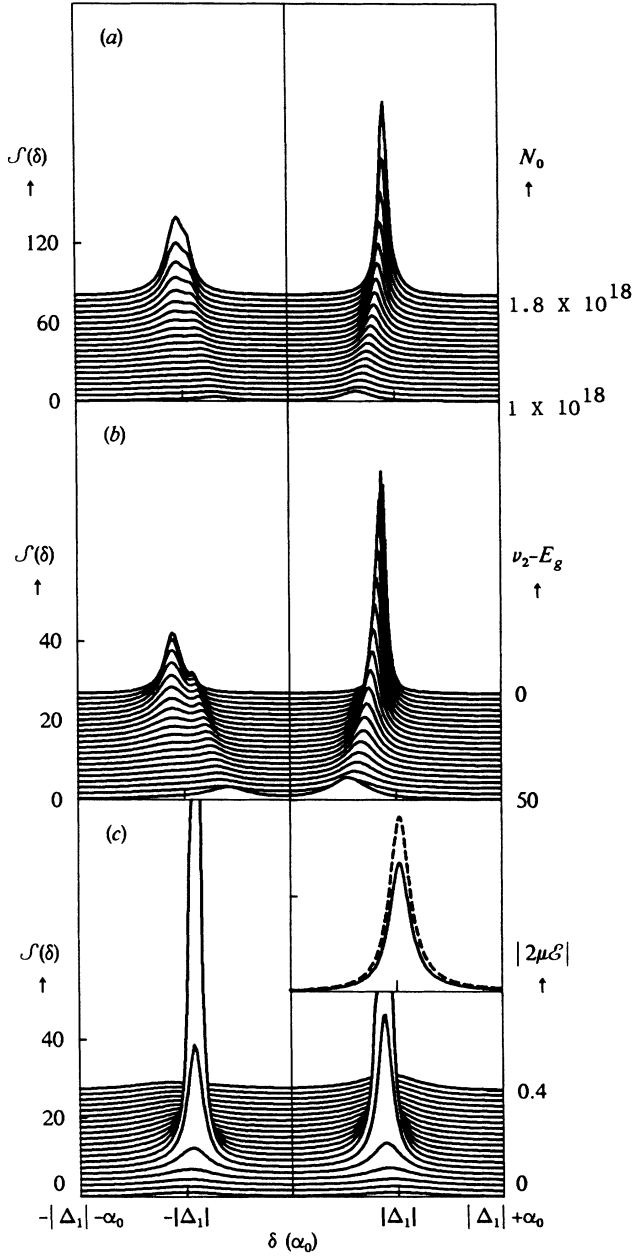


FIG. 8. Four-wave mixing spectrum in units of α_0^{-1} for (a) $\nu_2 - E_g = 40$ meV, $\Delta_1 = -0.001$ meV, $|2\nu\mathcal{E}| = 0.2$ meV, (b) $N_0 = 10^{18}$ cm $^{-3}$, $\Delta_1 = -0.002$ meV, $|2\nu\mathcal{E}| = 0.2$ meV, (c) $N_0 = 10^{18}$ cm $^{-3}$, $\Delta_1 = -0.0001$ meV, $\nu_2 - E_g = 40$ meV. In (a) N_0 is given in units of cm $^{-3}$ and in (b) and (c) $\nu_2 - E_g$ and $|2\nu\mathcal{E}|$ are both given in meV. The rest of the parameters are the same as in Fig. 2. The inset in (c) shows the peak intensity vs the Rabi frequency where the solid line is for the low energy mode and the dashed line is for the high energy mode. The x axis of the inset ranges from 0.1 to 0.15 meV while the y axis ranges from 0 to 2800 α_0^{-1} .

As stated earlier, perfect phase matching cannot be achieved in a collinear cavity configuration due to the dispersive response of the medium. However, the external pump frequency may be adjusted at various intensities so that it is kept approximately resonant with the nonlinear dressed pumped cavity. This corresponds to a detuning of the pump mode from the passive-cavity mode equal to $\Delta\Omega = -\text{Im}[\tilde{\alpha}_1(\Delta_1=0)]$ which would seem to be the most straightforward way of maximizing the response of the internal cavity field to the external driving field. Several graphs of the NDFWM spectrum for this choice of $\Delta\Omega$ are shown in Fig. 8. In Figs. 8(a) and 8(b) we plot the output spectrum for increasing carrier density and decreasing pump frequency, respectively. Figure 8(a) shows that as the carrier density in the medium is increased, the sidemode intensity also increases. This reflects the fact that the absorption decreases while the background fluorescence δA_0 increases for increasing carrier densities. Figure 8(b) shows that as we increase the pump frequency far into the band, the output intensity decreases rapidly. This feature of the spectrum is also not very surprising since the absorption increases while the background fluorescence δA_0 decreases for increasing pump frequency. In addition, both of these graphs exhibit the same general feature that more light is emitted at $|\Delta_1|$ than at $-|\Delta_1|$. In the gain region the asymmetry reverses and the mode at $-|\Delta_1|$ has the greatest intensity. This feature has been observed in traveling wave amplifiers,¹⁸ and it is mainly due to the pump-induced asymmetry in the absorption spectra which cause the side modes to have different absorption and refractive index values.

In Fig. 8(c) we plot the output spectrum for increasing pump intensity which shows a resonant structure at $|2\nu\mathcal{E}| \cong 0.1$ meV. This feature is easily understood as the coinciding of the relaxation oscillation frequency with the cavity frequency $\pm|\Delta_1|$. The peak intensity of the sidemodes as a function of the Rabi frequency is shown in the inset of Fig. 8(c). As the pump intensity is increased the relaxation oscillation frequency passes through the cavity mode and the resonant feature disappears.

V. SQUEEZED STATES

In this section we wish to calculate the amount of squeezing from an intracavity FWM experiment using a semiconductor medium. Squeezed light results from a linear combination of the sideband amplitudes d_1 and d_3 . To detect squeezing, a homodyne detection scheme may be used wherein the sidemode fields exiting the cavity are mixed with a local oscillator whose phase is shifted an angle θ with respect to the strong mode ν_2 . The total amplitude d of the squeezed field is given by

$$d = d_1 e^{-i\theta} + d_3^\dagger e^{i\theta}. \quad (22)$$

From this operator we define two conjugate Hermitian operators

$$X_+ = d + d^\dagger, \quad X_- = i(d - d^\dagger). \quad (23)$$

The variance of an operator is defined to be the expect-

tation value of its square minus the square of its expectation value, so using the above definitions the variance of X_+ is

$$V(X_+) = 1 + \langle d_1^\dagger d_1 \rangle + \langle d_3^\dagger d_3 \rangle + \langle d_1 d_3 \rangle e^{-2i\theta} + \langle d_1^\dagger d_3^\dagger \rangle e^{2i\theta}, \quad (24)$$

where squeezing occurs for $V(X_+) < 1$ and perfect squeezing corresponds to $V(X_+) = 0$. However, Eq. (24) only describes the squeezing inside the cavity whereas a detector outside the cavity sees a non- δ -function spectrum around each cavity mode frequency due to the fluctuations. Therefore, in order to find the squeezing outside of the cavity we simply replace the expectation values with the corresponding spectral quantities. Furthermore, as noted by Collett and Gardiner^{19,20} these spectral quantities are modified by the density of states factor $2\gamma_{\text{cav}}$ describing the transmission through the cavity mirror.

$$V(X_+) = 1 + \gamma_{\text{cav}} (\mathcal{S}_{12}(\delta) + \mathcal{S}_{21}(\delta) + \mathcal{S}_{34}(\delta) + \mathcal{S}_{43}(\delta) + \{[\mathcal{S}_{13}(\delta) + \mathcal{S}_{31}(\delta)]e^{-2i\theta} + \text{c.c.}\}), \quad (25)$$

where we have taken the optimal situation of a single-port cavity. Since the angle θ is not restricted we may choose it in such a way as to achieve maximum squeezing. The best squeezing is

$$V(X_+) = 1 + \gamma_{\text{cav}} [\mathcal{S}_{12}(\delta) + \mathcal{S}_{21}(\delta) + \mathcal{S}_{34}(\delta) + \mathcal{S}_{43}(\delta) - 2|\mathcal{S}_{13}(\delta) + \mathcal{S}_{31}(\delta)|], \quad (26)$$

where θ is chosen such that

$$\cos(2\theta) = \frac{\text{Re}(\mathcal{S}_{13} + \mathcal{S}_{31})}{|\mathcal{S}_{13} + \mathcal{S}_{31}|}, \quad \sin(2\theta) = \frac{\text{Im}(\mathcal{S}_{13} + \mathcal{S}_{31})}{|\mathcal{S}_{13} + \mathcal{S}_{31}|}. \quad (27)$$

In Fig. 9 we plot the squeezing spectrum in the output field for θ given by Eq. (27). Figures 9(a) and 9(b) both

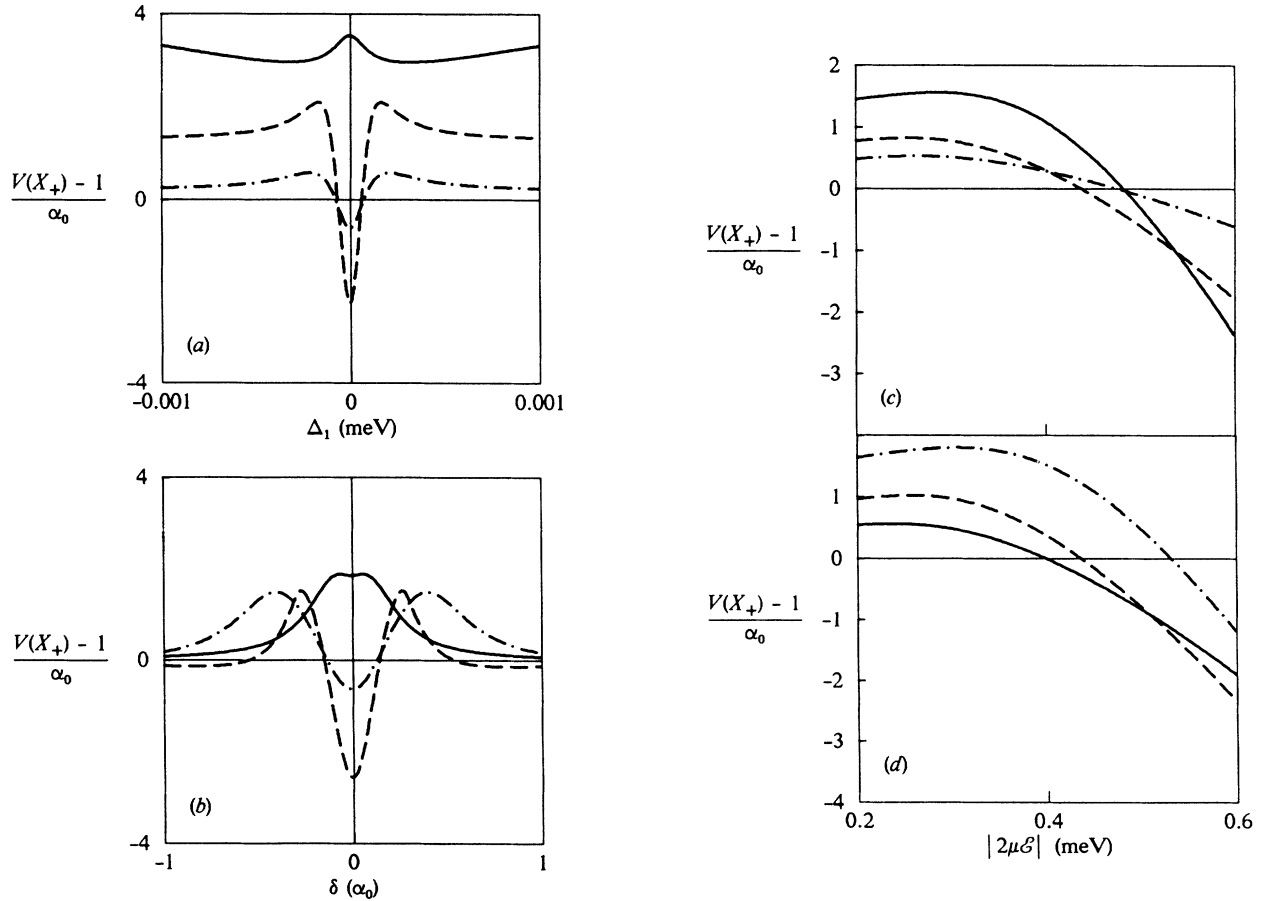


FIG. 9. Variance with respect to the vacuum $[V(X_+) - 1]/C$ where the cooperativity $C = g^2/\gamma_{\text{cav}}\gamma$. (a) $\delta = 0$, $|\mu\mathcal{E}| = 0.3$ meV, $N_0 = 10^{18}$ cm⁻³, $\nu_2 - E_g = 10$ meV (solid), 45 meV (dashed), 80 meV (dot-dashed); (b) $\Delta_1 = 0$, $|\mu\mathcal{E}| = 0.3$ meV, $N_0 = 10^{18}$ cm⁻³, $\nu_2 - E_g = 30$ meV (solid), 50 meV (dashed), 80 meV (dot-dashed); (c) $\delta = 0$, $\Delta_1 = 0$, $N_0 = 10^{18}$ cm⁻³, $\nu_2 - E_g = 50$ meV (solid), 65 meV (dashed), 80 meV (dot-dashed); (d) $\delta = 0$, $\Delta_1 = 0$, $\nu_2 - E_g = 60$ meV, $N_0 = 8 \times 10^{17}$ cm⁻³ (solid), 10^{18} cm⁻³ (dashed), 1.2×10^{18} (dot-dashed) cm⁻³.

suggest that by saturating the medium in a DFWM scheme one can overcome the phase-insensitive fluorescence enough to produce squeezing. As mentioned earlier we expected a DFWM or nearly DFWM scheme to produce the best squeezing result because of the narrow spectrum of the phase-sensitive noise term C_1 . In addition, Fig. 9(b) shows why the use of a cavity is beneficial in the production of squeezed light. Remembering that $\langle d_1^\dagger d_1 \rangle$ is the spectral average of $\mathcal{S}_{21}(\delta)$, then we see that the variance given by Eq. (24) is the average of that in Fig. 9(b). Keeping these facts in mind we set $\delta=0$ and $\Delta_1=0$ and plot the variance versus pump intensity in Figs. 9(c) and 9(d). From both of these figures we conclude that the best squeezing is obtained near threshold $N_0 \cong 10^{18} \text{ cm}^{-3}$ at about 50 meV above the bandgap. However, since these plots are in units of the inverse of the cooperativity, it would appear that the best squeezing occurs in the low- Q cavity limit, which however, cannot be treated consistently in the present formalism.

VI. CONCLUSION

We have presented a quantum theory of NDFWM for a highly excited semiconductor in a cavity. Our theory assumes small intensity fluctuations and our equations are linear in the sidemode amplitudes. Hence, we do not take into account any feedback effects of the sideband intensities on the pump. We have calculated the effect of the strong mode on the sidemode absorption spectrum and the resonance fluorescence spectrum. Our results show that these quantities are greatly modified in the spectral region around the pump, leading to an enhancement of the NDFWM spectrum. The absorption coefficient as well as the resonance fluorescence shows a pronounced asymmetric dip for large enough pump intensities. Furthermore, we have found that the asymmetry in NDFWM spectrum is a result of the corresponding asymmetry in the absorption coefficient and the dispersive response of the system. The features predicted have their origin in the scattering of the pump field into the sidemodes by the carrier density fluctuations. We compute the squeezing in the sidemode spectrum for a NDFWM intracavity experiment. Our analysis shows that a DFWM scheme results in the greatest amount of squeezing. This feature arises because of the similarity in the noise terms C_1 and A_1 .

ACKNOWLEDGMENTS

This work was supported in part by the U.S. Army Research Office and the U.S. Air Force Office of Scientific Research (JSOP), in part by the U.S. Office of Naval Research, in part by the Optical Circuitry Cooperative at the Optical Sciences Center, and by a Sandia contract.

APPENDIX

In this appendix we derive the equations of motion for the semiconductor-field correlations. Because the semiconductor is assumed to be in the quasiequilibrium regime due to the rapid Coulomb scattering, the material

dynamics reach steady state nearly instantaneously. Therefore, the equations describing the material dynamics are solved in steady state and inserted into the FWM coefficients A_n , B_n , C_n , and D_n . As in the familiar two-level system, we find that the average photon number and the combination tone couple to expectation values containing various combinations of field and electron-hole operators. To simplify these coupled equations we introduce the following notation consistent with that of Lindberg *et al.*¹⁶

$$C_n(k) \equiv \langle d_n a_k^\dagger b_{-k}^\dagger \rangle, \quad D_n(k) \equiv \langle d_n b_{-k} a_k \rangle, \quad (\text{A1a})$$

$$E_n(k) \equiv \langle d_n a_k^\dagger a_k \rangle, \quad H_n(k) \equiv \langle d_n b_{-k}^\dagger b_{-k} \rangle, \quad (\text{A1b})$$

where $C_n(k)$ and $D_n(k)$ are the dipole-field correlations and $E_n(k)$ and $H_n(k)$ are the electron and hole population-field correlations.

A standard approach to solving these equations involves factorizing the weakest correlation from these expectation values by introducing a fluctuation operator $\hat{\delta}$:

$$\hat{\delta} \langle \hat{O}_f \hat{Q}_{e-h} \rangle = \langle \hat{O}_f \hat{Q}_{e-h} \rangle - \langle \hat{O}_f \rangle \langle \hat{Q}_{e-h} \rangle, \quad (\text{A2})$$

where \hat{O}_f and \hat{Q}_{e-h} symbolize field and electron-hole operators, respectively. Using this notation, we can rewrite Eqs. (A1a) and (A1b) as a factorized contribution plus a fluctuation contribution, i.e.,

$$C_n(k) = \langle d_n \rangle p^*(k) + \hat{\delta} C_n(k), \quad (\text{A3a})$$

$$D_n(k) = \langle d_n \rangle p(k) + \hat{\delta} D_n(k),$$

$$E_n(k) = \langle d_n \rangle f_e(k) + \hat{\delta} E_n(k), \quad (\text{A3b})$$

$$H_n(k) = \langle d_n \rangle f_h(k) + \hat{\delta} H_n(k),$$

where we have let $n_e(k) \rightarrow f_e(k)$ and $n_h(k) \rightarrow f_h(k)$ since the system is assumed to be in the quasiequilibrium region, where all electron-hole bound states are absent due to screening. It has been shown¹⁶ that in the quasiequilibrium regime the fluctuations of the individual k states are proportional to the total carrier density fluctuations in which case the following relations are valid under steady-state conditions

$$\hat{\delta} E_n(k) \cong g_e(k) \sum_k \hat{\delta} E_n(k) = g_e(k) \hat{\delta} E_n, \quad (\text{A4a})$$

$$\hat{\delta} H_n(k) \cong g_h(k) \sum_k \hat{\delta} H_n(k) = g_h(k) \hat{\delta} H_n, \quad (\text{A4b})$$

where the coefficients $g_e(k)$ and $g_h(k)$ are the leading coefficients of a Taylor series given by the equation ($\alpha=e,h$)

$$g_\alpha(k) = \frac{\partial f_\alpha(k)}{\partial \mu_\alpha} \frac{\partial \mu_\alpha}{\partial N_\alpha} = \frac{f_\alpha(k)[1-f_\alpha(k)]}{V^{-1} \sum_{k'} f_\alpha(k')[1-f_\alpha(k')]} \quad (\text{A4c})$$

The total carrier-density pulsations $\hat{\delta} E_n$ and $\hat{\delta} H_n$ are analogous to the semiclassical population pulsations, and the quasiequilibrium Eqs. (A4a) and (A4b) illustrate the fact that the field is correlated with the electron-hole excitations through the total number of carriers or

equivalently the chemical potentials.

Next we derive the equations of motion for $\hat{\delta}C_n(k)$, $\hat{\delta}D_n(k)$, $\hat{\delta}E_n$, and $\hat{\delta}H_n$. It is straightforward to show that the equation for $\langle d_n \rangle$ is not coupled to the equations for $\hat{\delta}C_n(k)$, $\hat{\delta}D_n(k)$, $\hat{\delta}E_n$, and $\hat{\delta}H_n$. Therefore, we calculate it separately, and it only contributes to the factorized part of $C_n(k)$ and $D_n(k)$, i.e., to the zeroth order of $\langle d_1^\dagger d_1 \rangle$ and $\langle d_1 d_3 \rangle$. In addition, since the side modes are assumed to be weak, we may take $g(k)$ as a small parameter and drop terms higher than second order in $g(k)$. Furthermore, we assume that the correlations to factorization of the field and electron-hole variables only

give rise to higher-order effects in $g(k)$ which can be neglected. Therefore, we ignore correlations like $\langle (d_n)^m Q_{e-h} \rangle$ when m is greater than one, so that the equations of motion for the fluctuations are derived from the equation of motion for $\langle d_n \rangle$:

$$\frac{d}{dt} \langle d_n \rangle = -(2\gamma_{\text{cav}} + i\Delta_n) \langle d_n \rangle + i \sum_k g^*(k) p(k), \quad (\text{A5})$$

where Δ_n is the detuned frequency $\nu_n - \nu_2$.

In these approximations, we obtain the following equations of motion for the fluctuations:

$$\begin{aligned} \frac{d}{dt} \hat{\delta}C_n(k) = & -\{\gamma - i[\omega(k) - \Delta_n]\} \hat{\delta}C_n(k) + i\mu_k^* \mathcal{E}^* [g_e(k) \hat{\delta}E_n + g_h(k) \hat{\delta}H_n] \\ & - ig^*(k) \{ [1 - f_e(k) - f_h(k)] \langle d_n^\dagger d_n \rangle - f_e(k) f_h(k) \}, \end{aligned} \quad (\text{A6a})$$

$$\begin{aligned} \frac{d}{dt} \hat{\delta}D_n(k) = & -\{\gamma + i[\omega(k) + \Delta_n]\} \hat{\delta}D_n(k) - i\mu_k \mathcal{E} [g_e(k) \hat{\delta}E_n + g_h(k) \hat{\delta}H_n] \\ & + ig(k) [1 - f_e(k) - f_h(k)] \langle d_1 d_3 \rangle - ig^*(k) [p(k)]^2, \end{aligned} \quad (\text{A6b})$$

$$\begin{aligned} \frac{d}{dt} \hat{\delta}E_n = & -\left[i\Delta_n + \gamma_{\text{NR}} + \Gamma \sum_k g_e(k) f_h(k) \right] \hat{\delta}E_n - \Gamma \sum_k g_h(k) f_e(k) \hat{\delta}H_n + i \sum_k \mu_k \mathcal{E} \hat{\delta}C_1(k) - i \sum_k \mu_k^* \mathcal{E}^* \hat{\delta}D_1(k) \\ & + \sum_k \mu_k \mathcal{E} g^*(k) \mathcal{D}_2^*(k) \{ [1 - f_e(k) - f_h(k)] \langle d_n^\dagger d_n \rangle - f_e(k) f_h(k) \} \\ & + \sum_k \mu_k^* \mathcal{E}^* g(k) \mathcal{D}_2(k) [1 - f_e(k) - f_h(k)] \langle d_1 d_3 \rangle + \sum_k \mu_k \mathcal{E} g^*(k) \mathcal{D}_2^*(k) [1 - f_e(k)] f_e(k), \end{aligned} \quad (\text{A6c})$$

and the equation for $\hat{\delta}H_n$ is given by Eq. (A6c) with $\hat{\delta}E_n$ interchanged with $\hat{\delta}H_n$ and e interchanged with h . The last term in Eq. (A6c) reflects the fact that the fluctuations of electrons and holes in their quasithermal distributions are uncorrelated.

These equations may be simplified since for the small pump-probe detunings under consideration we can rewrite the complex Lorentzian as

$$\mathcal{D}_2(\omega(k) \pm \Delta_n) \cong \mathcal{D}_2(k) \pm i\Delta_n [\mathcal{D}_2(k)]^2 \cong \mathcal{D}_2(k). \quad (\text{A7})$$

If we use this approximation then we can solve these equations in steady state to obtain

$$\hat{\delta}C_n(k) = i\mu_k^* \mathcal{E}^* \mathcal{D}_2(k) [g_e(k) \hat{\delta}E_n + g_h(k) \hat{\delta}H_n] - ig^*(k) \mathcal{D}_2(k) \{ [1 - f_e(k) - f_h(k)] \langle d_n^\dagger d_n \rangle - f_e(k) f_h(k) \}, \quad (\text{A8a})$$

$$\begin{aligned} \hat{\delta}D_n(k) = & -i\mu_k \mathcal{E} \mathcal{D}_2^*(k) [g_e(k) \hat{\delta}E_n + g_h(k) \hat{\delta}H_n] + ig(k) \mathcal{D}_2^*(k) [1 - f_e(k) - f_h(k)] \langle d_1 d_3 \rangle \\ & + i\mu_k^2 \mathcal{E}^2 g^*(k) [\mathcal{D}_2^*(k)]^3 [1 - f_e(k) - f_h(k)]^2. \end{aligned} \quad (\text{A8b})$$

Substituting these solutions into Eq. (A6c) leads to the steady-state solution

$$\begin{aligned} \hat{\delta}E_n = & \sum_k \frac{2\mu_k \mathcal{E} g^*(k)}{(\gamma_{\text{NR}} + \gamma_e + \gamma_h + i\Delta_n)} \frac{\mathcal{L}(k)}{\gamma} \{ [1 - f_e(k) - f_h(k)] \langle d_n^\dagger d_n \rangle - f_e(k) f_h(k) \} \\ & + \sum_k \frac{2\mu_k^* \mathcal{E}^* g(k)}{(\gamma_{\text{NR}} + \gamma_e + \gamma_h + i\Delta_n)} \frac{\mathcal{L}(k)}{\gamma} [1 - f_e(k) - f_h(k)] \langle d_1 d_3 \rangle \\ & + \sum_k \frac{|\mu_k \mathcal{E}|^2 \mu_k \mathcal{E} g^*(k)}{(\gamma_{\text{NR}} + \gamma_e + \gamma_h + i\Delta_n)} \mathcal{D}_2^*(k)^3 [1 - f_e(k) - f_h(k)]^2 \\ & + \frac{\gamma_{\text{NR}} + \gamma_e + i\Delta_n}{(\gamma_{\text{NR}} + \gamma_e + \gamma_h + i\Delta_n)(\gamma_{\text{NR}} + i\Delta_n)} \sum_k \mu_k \mathcal{E} g^*(k) \mathcal{D}_2^*(k) [1 - f_e(k)] f_e(k) \\ & - \frac{\gamma_e}{(\gamma_{\text{NR}} + \gamma_e + \gamma_h + i\Delta_n)(\gamma_{\text{NR}} + i\Delta_n)} \sum_k \mu_k \mathcal{E} g^*(k) \mathcal{D}_2^*(k) [1 - f_h(k)] f_h(k), \end{aligned} \quad (\text{A8c})$$

where $\mathcal{L}(k) = \gamma \text{Re}[D_2(k)]$ and we have introduced the scattering rates

$$\gamma_\alpha = \Gamma \sum_k f_\alpha(k) g_{\alpha'}(k) + \sum_k 2|\mu_k \mathcal{E}|^2 \frac{\mathcal{L}(k)}{\gamma} g_{\alpha'}(k), \quad (\text{A8d})$$

with $\alpha, \alpha' = e, h$, and $\alpha' \neq \alpha$. The sum $\gamma_{\text{NR}} + \gamma_e + \gamma_h$ is sometimes referred to as the power-broadened carrier-density decay constant. Again we obtain the steady-state equation for $\hat{\delta}H_n$ by making the replacements $\hat{\delta}E_n \leftrightarrow \hat{\delta}H_n$ and $e \leftrightarrow h$. In Eq. (A8a) the last term proportional to $g(k)$ is independent of the pump field and is essentially determined by the Fermi-Dirac distributions. This is also true for the second term in Eq. (A8b). These contributions are obtained regardless of the excitation mechanism for the semiconductor. On the other hand, the first terms in Eqs. (A8a) and (A8b) are proportional to the carrier-density pulsations $\hat{\delta}E_n$ and $\hat{\delta}H_n$, and it is exactly these terms that give rise to the coherent modification of the FWM coefficients.

Using the density matrix formalism of Eq. (2) along

with the definitions (A1a) and (A1b) we can begin to write down the equation of motion for $\langle d_1^\dagger d_1 \rangle$ and $\langle d_1 d_3 \rangle$

$$\frac{d}{dt} \langle d_1^\dagger d_1 \rangle = - \left[i \sum_k g(k) C_1(k) + \text{c.c.} \right] - 2\gamma_{\text{cav}} \langle d_1^\dagger d_1 \rangle, \quad (\text{A9a})$$

and

$$\frac{d}{dt} \langle d_1 d_3 \rangle = i \sum_k g^*(k) [D_1(k) + D_3(k)] - 2\gamma_{\text{cav}} \langle d_1 d_3 \rangle, \quad (\text{A9b})$$

where the equation for $\langle d_3^\dagger d_3 \rangle$ is given by Eq. (A9a) with the index 1 interchanged with 3. It is a tedious but straightforward task to substitute the steady-state solutions for $C_n(k)$ and $D_n(k)$ into Eqs. (A9a) and (A9b). After this is done a simple comparison with Eqs. (13a) and (13b) leads to the definitions of the coefficients A_n , B_n , C_n , and D_n .

¹H. P. Yuen and J. H. Shapiro, *Opt. Lett.* **4**, 334 (1979).

²B. Yurke, *Phys. Rev. A* **32**, 300 (1985).

³M. D. Reid and D. F. Walls, *Phys. Rev. A* **34**, 4929 (1986).

⁴D. A. Holm and M. Sargent III, *Phys. Rev. A* **35**, 2150 (1987).

⁵M. Sargent III, F. Zhou, and S. W. Koch, *Phys. Rev. A* **38**, 4673 (1988).

⁶F. Zhou, M. Sargent III, S. W. Koch, and W. Chow, *Phys. Rev. A* **41**, 463 (1990).

⁷G. P. Agrawal, *J. Opt. Soc. Am. B* **5**, 147 (1988).

⁸H. Haug and S. Schmitt-Rink, *Prog. Quantum Electron.* **9**, 3 (1984).

⁹*Optical Nonlinearities and Instabilities in Semiconductors*, edited by H. Haug (Academic, New York, 1988).

¹⁰S. W. Koch, N. Peyghambarian, and H. M. Gibbs, *J. Appl. Phys. (Rev.)* **63**, 1 (1988).

¹¹S. W. Koch, N. Peyghambarian, and M. Lindberg, *J. Phys. C*

21, 5229 (1988).

¹²M. Sargent III, D. A. Holm, and M. S. Zubairy, *Phys. Rev. A* **31**, 3112 (1985).

¹³M. Lindberg and S. W. Koch, *Phys. Rev. B* **38**, 3342 (1988).

¹⁴B. R. Mollow, *Phys. Rev.* **188**, 1969 (1969).

¹⁵For a review see, e.g., M. Sargent III, M. Scully, and W. E. Lamb, *Laser Physics* (Addison-Wesley, Reading, MA, 1977).

¹⁶M. Lindberg, S. An, S. W. Koch, and M. Sargent III, *Phys. Rev. A* **40**, 4415 (1989).

¹⁷M. Lax, *Rev. Mod. Phys.* **38**, 541 (1966).

¹⁸K. Inoue, T. Mukai, and T. Saitoh, *Appl. Phys. Lett.* **51** (14) (1987).

¹⁹M. J. Collett and C. W. Gardiner, *Phys. Rev. A* **30**, 1386 (1984).

²⁰C. W. Gardiner and M. J. Collett, *Phys. Rev. A* **31**, 3761 (1985).